I&EC research
Industrial & Engineering Chemistry Research

pubs.acs.org/IECR
Article

Effect of Organic Vapors on the Behavior of Air Bubbles in Solutions of Nonionic and Ionic Surfactants

Dominik Kosior,* Georgi Gochev, Piotr Batys, Łukasz Witkowski, Klaudia W. Zaręba, Piotr Warszyński, and Jan Zawala

Cite This: *Ind. Eng. Chem. Res.* 2025, 64, 20347−20361

ABSTRACT: We explored the physicochemical aspects of the problem of a rising air bubble in an aqueous surfactant solution, where saturated *n*-hexane vapor is present within the bubble. The rising velocity profiles of these bubbles were measured in pure water and salt-free solutions of a nonionic (*n*-octanol) or cationic (dodecyltrimethylammonium bromide, C_{12}TAB) surfactant at various concentrations. They were compared with the results for corresponding hexane-free systems. Additionally, dynamic surface tension for stationary bubbles was measured using bubble profile analysis tensiometry. To support these experimental data, we conducted an investigation using molecular dynamics (MD) simulations. For pure water, both surface tension measurements and MD simulations confirmed the adsorption of *n*-hexane molecules from the vapor phase to the stationary water interface, which is consistent with the literature reports. However, the rising bubble velocity was not affected by *n*-hexane vapor. We discuss this intriguing finding within the context of hydrodynamic forces. In the surfactant systems, a strong effect of coadsorption of surfactant from the solution and *n*-hexane from the vapor phase was observed in all investigations. The surface tension isotherms were theoretically described using a modified Frumkin adsorption model, additionally accounting for the ionic nature of C_{12}TAB and the coadsorption of *n*-hexane from the vapor. The free energy of adsorption exhibited a strong correlation with the free energy profiles at the interface, as determined by MD simulations. The rising bubble data were theoretically analyzed in terms of the drag coefficient and the extent of bubble deformation. However, studies of the bubble velocity profiles revealed some unusual features, particularly during the dynamic layer formation phase.

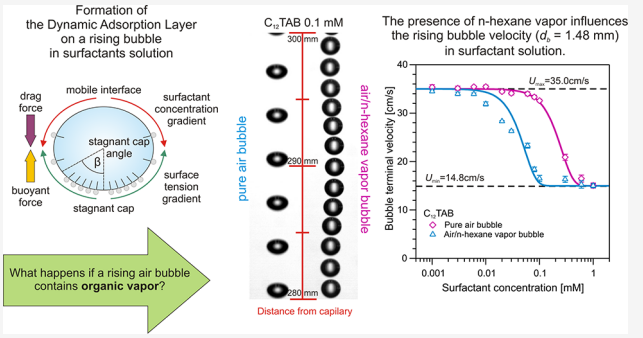

1. INTRODUCTION

Bubble motion is one of the key topics in fluid dynamics and plays a crucial role in mass transfer applications, thereby related processes are of importance to the chemical engineering of liquid/gas systems.[1,2] The presence of certain impurities on the bubble interface, originating from the liquid and/or gaseous phase, may affect its motion[3] and the formation and stability of the thin liquid film formed during bubble interactions with various interfaces.[4,5] Adsorption of molecules from aqueous solutions to a liquid/gas or a liquid/liquid interface can be described by adsorption dynamics models that have been applied to a plethora of experimental data.[6] An alternative scenario for liquid/gas interfaces is the adsorption of molecules from the gaseous phase. In the second half of the 20th century, this topic attracted scientific attention, as evidenced by several representative works[7−11] and more recent publications.[12−19] The main scientific approach was analysis of measurements of the decrease of surface tension γ (rise of surface pressure Π) due to adsorption of organic molecules at the water/vapor interface as a function of the partial vapor pressure P up to the saturation pressure P_0, usually at atmospheric ambient pressure, but, however, also at elevated ambient pressures.[9] Such $\Pi(P)_T$ isotherms were usually treated theoretically by the Gibbs adsorption equation in order to obtain the adsorbed amount.

The above-mentioned studies on pure water, as well as investigations of coadsorption from surfactant solutions and organic vapors, were further advanced by Miller and co-workers.[14−19] They demonstrated that adsorption of volatile organic molecules at the surfactant solution/vapor interface proceeds through four regimes.[19] In the absence of surfactants, the two liquid phases form a clean interface. At very low surfactant concentrations, much lower than at the surfactant

Received: June 26, 2025
Revised: September 30, 2025
Accepted: September 30, 2025
Published: October 10, 2025

https://doi.org/10.1021/acs.iecr.5c02608
Ind. Eng. Chem. Res. 2025, 64, 20347−20361

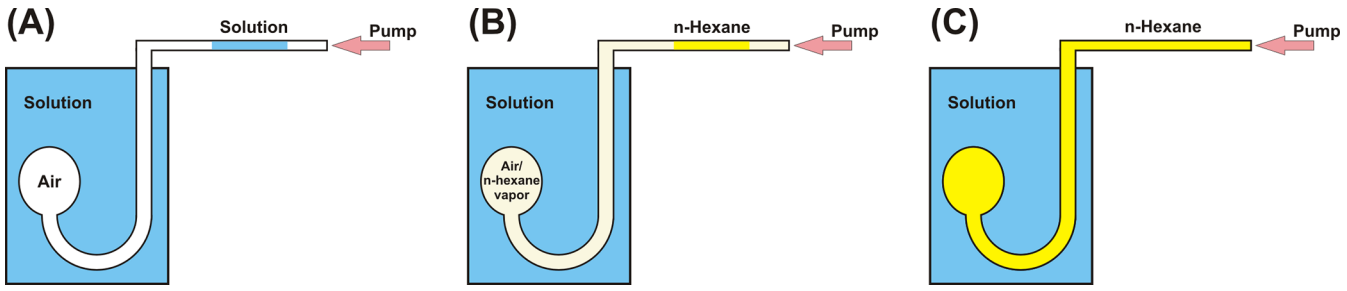

Figure 1. Schematic of interface tension measurements for (A) water−air (W/A) and surfactant solution−air (S/A) interfaces, (B) water−air/*n*-hexane vapor (W/V) and surfactant solution−air/*n*-hexane vapor (S/V) interfaces and (C) water−liquid *n*-hexane (W/H) and surfactant solution−liquid *n*-hexane (S/H) interfaces.

solution/pure air interface due to interactions with the oil phase, oil molecules cluster around the adsorbed surfactants, markedly reducing interfacial tension (cooperativity). With increasing concentration, surfactants progressively displace the oil molecules from the interface (competition), until at sufficiently high concentrations only a surfactant layer remains.

The problem of the adsorption/desorption process at the water/organic vapor interface was further explored using poorly soluble organic amphiphiles.[20,21] Extensive studies on volatile amphiphiles have demonstrated that their adsorption−desorption dynamics differ fundamentally from those of classical surfactants: adsorption from the vapor phase proceeds rapidly under mixed barrier−diffusion control, whereas desorption is typically governed by convection-enhanced mechanisms.[22,23] Dynamic tensiometry further revealed that adsorption from vapor dominates over liquid-side adsorption, making volatile surfactants effective "temporal" regulators of interfacial tension and foam stability.[24]

A more practical perspective on this phenomenon was presented by Drenckhan and co-workers in their studies on foam formation and stability in the presence of organic vapors.[25,26] They demonstrated that poorly water-soluble organic vapors, such as fluorocarbons, strongly enhance foam stability. These vapors suppress coarsening by hindering gas transfer through aqueous films, thereby establishing an osmotic pressure that counterbalances Laplace pressure differences. In addition, fluorocarbon vapors slow down coalescence by coadsorbing with surfactants at the gas/water interface, leading to mixed interfacial layers or even macroscopic vapor films at saturation. Consequently, even at low concentrations, fluorocarbon vapors extend foam lifetimes and provide a versatile means of controlling foam formation under dynamic conditions. Similar effects have been observed for solubilized flavor oils,[27,28] which can coadsorb with surfactants at the gas/water interface and thereby influence foam formation and stability. These findings show that organic additives, whether present as vapors or solubilized oils, can act as efficient regulators of foam formation and lifetime.

In this study, we extend the problem of adsorption of organic molecules from the vapor phase at a stationary liquid/gas interface to the case of a nonstationary interface, namely that of a rising bubble in surfactant solution.

In pure liquids, the rising bubble velocity depends on bubble diameter and the viscosity and density of the continuous phase; a fluid sphere can reach terminal velocities up to 50% higher than a rigid sphere of the same size due to internal gas circulation.[29] In surfactant solutions, adsorption at the bubble surface reduces interfacial mobility, lowering velocity.[3,4] This results from uneven surfactant distribution: depletion at the front and accumulation at the rear create a stagnant cap, inducing Marangoni stresses that oppose flow. The resulting dynamic adsorption layer (DAL), characterized by a concentration gradient along the bubble surface, is commonly described by the stagnant cap angle, which has been used in theoretical modeling,[30−32] with the general conclusion that an increase in the stagnant cap angle leads to a decrease in the bubble's terminal velocity.

Unfortunately, there is no direct experimental method to observe the formation and structure of the dynamic adsorption layer; therefore, indirect methods based on monitoring bubble motion or its collision with various interfaces are employed for this purpose.[33,34]

Bubble motion in a liquid can be divided into several characteristic stages, which can be revealed by determining the bubble local velocity profiles (LVPs).[3] In a clean liquid, a bubble detaches from the capillary orifice, accelerates, and attains its terminal velocity. However, in a solution containing surfactants, the motion consists of four distinct stages: acceleration, peak velocity, deceleration, and terminal velocity. Moreover, there is a minimum degree of adsorption coverage (concentration) that is required to fully immobilize the bubble. Further increase in adsorption coverage above this 'threshold' level has little to no effect on the bubble's terminal velocity.[3,4]

While the adsorption of organic vapors on water and surfactant solutions has attracted significant interest in the context of stationary drops[14,15] or bubbles,[12] only a very few studies have explored dynamic conditions, such as the cases of a growing bubble,[7,18] and particularly, a rising bubble in solution.[35] This paper presents a detailed analysis of the influence of saturated *n*-hexane vapor on some key interfacial characteristics of bubbles in aqueous surfactant solutions under both static and dynamic conditions.

2. MATERIALS AND METHODS

2.1. Materials. Dodecyltrimethylammonium bromide (C_{12}TAB, Sigma-Aldrich, ≥98%), *n*-octanol (Sigma-Aldrich, ≥98%), and *n*-hexane (Sigma-Aldrich, > 95%) used in the experiments were commercially available reagents. While *n*-octanol and *n*-hexane were used as received, C_{12}TAB was recrystallized three times from acetone containing traces of ethanol (analytical grade solvents). Ultrapure Milli-Q water (Merck Millipore, with resistivity of 18 MΩ·cm at 25 °C) was used without the addition of any electrolytes. Consequently, the ionic strength of *n*-octanol solutions was negligible, whereas for C_{12}TAB solutions, the ionic strength was determined by the surfactant molar concentration, c_S, assuming C_{12}TAB was fully ionized in solution.

https://doi.org/10.1021/acs.iecr.5c02608
Ind. Eng. Chem. Res. 2025, 64, 20347−20361

All experiments in this study were carried out at room temperature, approximately 24 ± 1 °C.

2.2. Methods. *2.2.1. Surface Tension of Stationary Bubbles.* Dynamic surface tension $\gamma(t)$ measurements were performed with a bubble profile analysis tensiometer PAT-1 (Sinterface Technologies, Germany); the γ-values were measured with an accuracy of about ± 0.15 mN/m. Details about the method can be found in previous work.[36] An air bubble was formed at the tip of a U-shaped steel capillary of 1 mm inner and 2 mm outer diameters immersed in a standard glass cuvette filled with ca. 23 mL of aqueous surfactant solution. The tubing connected to the capillary was partially filled with ca. 100 μL of water in the manner shown in Figure 1A). This way, the air bubble was in equilibrium with saturated water vapor in a gas reservoir of ca. 300 μL (bubble volume is ≈7.1 μL with corresponding surface area of ≈17 mm^2). Figure 1B shows a scheme of an equivalent experiment, but here, the water in the tubing was replaced by liquid *n*-hexane; this way, the air bubble was exposed to *n*-hexane/water vapors. Hereafter, the water/air interfaces without and with *n*-hexane vapor are denoted as W/A and W/V, respectively, while the surfactant solution/air interfaces without and with *n*-hexane vapor are denoted as S/A and S/V, respectively. In such an experiment, right after sucking liquid *n*-hexane into the tubing, it was quickly connected to the empty capillary. Then, the capillary was immersed in the solution, and a fresh bubble (hereafter called the '1st' bubble) was immediately formed, and surface tension measurement started. Such a '1st' bubble was initially not in equilibrium with saturated *n*-hexane/water vapors. Hence, with the gradual increase of *n*-hexane vapor pressure until saturation, we could monitor the change in the dynamic surface tension of the bubble. For a typical tubing length (L_t) of 20−30 cm and a gas-phase diffusion coefficient (D_c) of *n*-hexane in air of 8 × 10^{-5} m^2/s, the estimated diffusion time ($t_{diff} = L_t^2/D_c$) is on the order of 8−19 min, consistent with the ∼15 min time scale for surface tension stabilization. Accordingly, the second and subsequent bubbles were formed when the gas phase was already saturated with *n*-hexane vapors. The interface tension measurement time scale was up to 8 h, depending on the stabilization of the adsorption process. Once vapor saturation was established in the gas reservoir (after ca. 20 min), a couple of subsequent bubbles ('2nd', '3rd' bubble, etc.) were formed, and their $\gamma(t)$ dependence was measured, showing overlap dependence within experimental uncertainty.

The obtained data were used to construct the surface tension isotherms $\gamma(c_S)$, which can also be presented in terms of the surface pressure, $\Pi = \gamma_0 - \gamma$, where γ_0 is the surface tension of pure water against the gas phase, for water vapor in air $\gamma_0^{W/A} = 72.0 \pm 0.2$ mN/m. As discussed in detail in Section 3.1, this value changes in the presence of saturated *n*-hexane vapor. In this case, the surface tension of water against mixed water/*n*-hexane saturated vapors in air was $\gamma_0^{W/V} = 68.3 \pm 0.3$ mN/m. Additionally, comparative interfacial tension measurements were performed using liquid *n*-hexane drops in surfactant solutions. The interfacial tension between liquid *n*-hexane and pure water was measured to be $\gamma_0^{W/H} = 52.0 \pm 0.2$ mN/m. Hereafter, the water/liquid *n*-hexane interface and the surfactant solution/liquid *n*-hexane interface are denoted as W/H and S/H, respectively. In the whole following discussion, surface tension γ and surface pressure Π are used interchangeably.

The obtained experimental surface tension isotherms $\gamma(c_S)$ were theoretically treated using an adsorption model that considers the coadsorption of *n*-hexane from the vapor.

For the nonionic surfactant (*n*-octanol), we used the Frumkin isotherm with the modification accounting for the presence of *n*-hexane adsorbed layer:[6]

$$\frac{c_S}{\alpha_S}(1 - \theta_S - \theta_H) = \theta_S \exp[-2H_S\theta_S] \tag{1}$$

where α_S is the 'surface activity' of the surfactant, which is a measure of the free energy of the adsorption; $\theta_S = \Gamma_S/\Gamma_{S\infty}$ is the relative surfactant surface concentration, where Γ_S is the excess surface concentration of surfactant, and $\Gamma_{S\infty}$ is its limiting value for a closely packed monolayer; θ_H is the surface blocking parameter, which accounts for restricted geometrical and conformation freedom of hydrophobic chains of surfactant molecules penetrating *n*-hexane adsorbed layer; and H_S is the interaction parameter accounting for the attractive lateral interactions among the adsorbed surfactant hydrophobic chains. We emphasize that in the present analysis, the parameter θ_H is assumed constant, and this issue is discussed further below. Finally, we assumed that the adsorption layer of *n*-hexane at the interface of a stationary bubble is formed instantaneously for saturated vapor, as discussed further below in Section 3.1.

The adsorption of the cationic surfactant (C_{12}TAB) is described in terms of the extended 'surface quasi-two-dimensional electrolyte' (STDE) model, which, for the single charge surfactant in water, exploits the set of equations:[37,38]

$$\frac{a_S}{\alpha_S}\left(-\frac{e\psi_{St}}{kT}\right)(1 - \theta_S - \theta_C - \theta_H) = \theta_S \exp[-2H_S\theta_S]\exp\left(\frac{\phi_S}{kT}\right) \tag{2}$$

for surfactant cation (subscript '*S*'), and

$$\frac{a_C}{\alpha_C}\left(-\frac{e\psi_{St}}{kT}\right)(1 - \theta_S - \theta_C)^{g_{CS}} = \theta_C \exp\left(\frac{\phi_C}{kT}\right) \tag{3}$$

for surfactant counterion (subscript 'C'). Here, ψ_{St} is the electric potential of the Stern layer, k is the Boltzmann constant, $a_i = f_i c_i$ are the activities of surfactant ion and respective counterion in the solution, where f_i are activity coefficients, and c_i are molar concentrations. The activity coefficients f_i can be calculated using the extended Debye−Hückel theory.[39] The parameter α_S is the 'surface activity' of the surfactant cation, a measure of the adsorption's free energy after separating the electric components' contribution. The parameter α_C is the 'surface activity' of the surfactant counterion, which is a measure of their penetration into the Stern layer due to van der Waals interactions, image forces and hydration, $\theta_S = \Gamma_C/\Gamma_{C\infty}$ is the relative counterion concentration, where Γ_C is the surface excess concentration for surfactant counterion and $\Gamma_{S\infty}$ is its limiting surface concentration, and $g_{CS} = \Gamma_{S\infty}/\Gamma_{C\infty}$.

The electric potential of the Stern layer can be found using

$$\psi_{St} = \psi_d + \frac{\sigma\delta}{\varepsilon_0\varepsilon_{St}} \tag{4}$$

where δ is the thickness of the Stern layer, ε_0 is the vacuum permittivity, and ε_{St} is the dielectric constant of the Stern layer. The surface charge density σ and the diffuse layer potential ψ_d

https://doi.org/10.1021/acs.iecr.5c02608
Ind. Eng. Chem. Res. 2025, 64, 20347−20361

at the boundary between the Stern layer and the diffuse part of the electric double layer can be calculated as

$$\sigma = F(\Gamma_S - \Gamma_C) \tag{5}$$

$$\psi_d = \frac{2kT}{e}\sinh^{-1}\left(\frac{\sigma e}{2\varepsilon_0 \varepsilon kT\kappa}\right) \tag{6}$$

where F is the Faraday constant, e is the elementary charge, ε is the dielectric constant of the solution, and κ is the reciprocal Debye screening length. The activity corrections for the electrostatic interactions in the Stern layer, ϕ_i, for surfactant ion and counterion can be found from

$$\frac{\phi_i}{kT} = \frac{e^2}{8\pi\varepsilon_0\varepsilon kT}\frac{\kappa_S}{1 + \kappa_S r_{si}} \tag{7}$$

where r_{si} has the meaning of an effective ionic radius in the interfacial layer and κ_S is the two-dimensional surface equivalent of κ defined as[40]

$$\kappa_S = \frac{e^2}{\varepsilon_0\varepsilon kT}(\Gamma_S + \Gamma_C) \tag{8}$$

Further details of the STDE model can be found in previous works.[37,38,41,42]

The numerical procedure for the calculation of the theoretical surface tension isotherms $\gamma(c_S)$ is based on three steps:

(1) the solution of eq 1 for *n*-octanol or the system of eqs 2−8 for C_{12}TAB for the values of the surface concentrations $\Gamma_S(c_S)$ and $\Gamma_C(c_S)$
(2) substitution into the Gibbs adsorption equation
(3) fit to the experimental data for the respective surface tension isotherm. The fit quality was analyzed in terms of the parameter χ^2 defined as[38]

$$\chi^2 = \sum_{i=1}^{m}\frac{[\gamma_{ex}(c_i) - \gamma_{ev}(c_i)]^2}{f_g} \tag{9}$$

where $\gamma_{ex}(c_i)$ and $\gamma_{ev}(c_i)$ are the experimental and theoretically evaluated γ-values, respectively, m is the number of experimental points and $f_g = (m - n - 1)$ is the number of degrees of freedom with n being the number of fitting parameters.

2.2.2. Molecular Dynamics Simulations. The simulation protocol was described in our previous paper.[43] The Gromacs 2022.3 package,[44] with the CHARMM36 force field,[45] was used. Briefly, the CHARMM36-saturated lipid model was used for C_{12}TAB,[46] while the compatible CHARMM General Force Field was applied to *n*-octanol and *n*-hexane.[47] The structure and topology of molecules were generated using the CHARMM-GUI web server.[48] For water, the 4-point rigid water model, OPC4 was applied,[49] as it enables the reliable determination of surface tension.[50]

Molecular dynamics (MD) simulations at the air/water interface were performed using constant number of particles, volume, and temperature (NVT ensemble). Temperature coupling was controlled via a V-rescale thermostat at a temperature of 298 K and a coupling constant of 0.5 ps.[51] The van der Waals interactions were described by the Lennard-Jones potential, smoothly shifted to zero between 1.0 and 1.2 nm. The electrostatic interactions were modeled using the Partial Mesh Evald (PME) method,[52] with a 1.2 nm cutoff, 0.12 nm grid spacing, fourth-order splines, and a correction for the slab geometry.[53] In the case of C_{12}TAB, an adequate number of Br^- ions were added to make the simulation systems charge neutral in all simulations. The equations of motion were integrated using the leapfrog integration scheme and a 2 fs time step. Bonds involving hydrogen were constrained using LINCS and SETTLE algorithms.[54,55] The VMD software package was used for visualization purposes.[56]

A periodic rectangular simulation box with dimensions 8 × 8 × 24 nm^3 was used, containing a water slab approximately 8 nm thick, separated by a vacuum or *n*-hexane vapor region. Initial configurations, generated using PACKMOL,[57] were constructed by randomly placing surfactant molecules into two monolayers at opposite orientations. Surfactant headgroups were oriented toward the water slab, while the exact angle between the tail and the interface was chosen randomly. Amounts of surfactant on the surface were set arbitrarily to 50 molecules per surface, while the number of *n*-hexane molecules was 400. For both surfactants, two systems were investigated, i.e., with and without *n*-hexane vapor. We performed 200 steps of energy minimization followed by a 140 ns long production run. In the case of simulations with *n*-hexane vapor, the equilibration of the system was estimated based on the changes in the mass distribution profiles.

Separately, we determined the free energy of a single surfactant molecule desorption from an interface. The final configurations were used to compute a potential of mean force (PMF). First, the pulling simulation protocol was initiated. The force was applied to the center of the selected surfactant molecule in order to enforce its desorption from the interface to the bulk solution. The value for the corresponding force constant was 1000 kJ/mol/nm^2. The distance between the selected surfactant's center of mass and the interface was chosen as the reaction coordinate, along which 25−40 windows were selected, depending on the system. Free energy was calculated using the umbrella sampling procedure. The data within each window were collected every 10 ps for a duration of 10 ns per window. The free energy profiles were constructed with the weighted histogram analysis method as implemented in GROMACS (*gmx wham* tool).[58] Statistical uncertainties were estimated using the Bayesian bootstrapping of complete histograms.[59] For the sake of comparison between the systems, the free energy was set to 0.0 kJ at a separation distance of 2.5 nm.

2.2.3. Rising Bubble. Figure 2 schematically presents the setup of the rising bubble experiment. In brief, the experiment was conducted in a square borosilicate glass column (40 mm × 40 mm) with a height of 400 mm, filled with the studied surfactant solution. A capillary with an inner diameter of 0.075 mm was mounted at the bottom of the column. The capillary was connected to a gastight glass syringe (Hamilton, 5 mL) mounted in a vertically positioned, high-precision syringe pump. The mean time required for bubble formation at the capillary was determined to be approximately 1.6 s. A high-speed camera (SpeedCam MacroVis, 100 frames per second) was used to monitor bubble movement. For experiments with *n*-hexane vapor, 1 mL of *n*-hexane was placed inside the syringe and kept in contact for 30 min to ensure saturation. Both experiments, conducted with clean air and the air/*n*-hexane vapor system, were performed sequentially in the same surfactant solution to minimize experimental errors caused by additional solution preparation (dilution from the stock solution) and minor variations in surfactant concentration (c_S).

https://doi.org/10.1021/acs.iecr.5c02608
Ind. Eng. Chem. Res. 2025, 64, 20347−20361

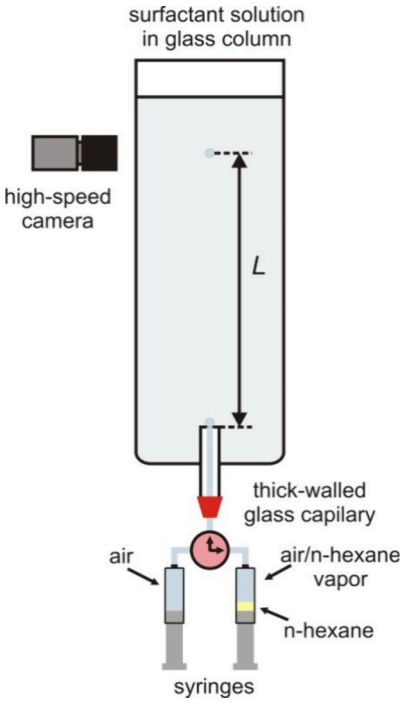

Figure 2. Schematic of the rising bubble setup.

To obtain absolute dimensions, an image of a nylon sphere with a diameter of 3.89 mm, inserted into the column after each experiment, was recorded.

The frame-by-frame analysis of the collected movies was automated by an in-house-written Python script (using OpenCV 3.4.13 and PIL 7.2.0 modules). The local velocity of the bubble (U_b) at a given position was calculated as

$$U_b = \frac{\sqrt{(x_i - x_{i-1})^2 + (y_i - y_{i-1})^2}}{\Delta t} \tag{10}$$

where (x, y) are the coordinates of the subsequent positions of the bubble, and Δt = 10 ms is the time interval between subsequent frames of the camera. As a rising bubble deforms, its size is characterized by the equivalent diameter (d_{eq}), defined as the diameter of a sphere having the same volume as the bubble. By approximating the bubble as an oblate spheroid with a horizontal diameter (d_h) and a vertical diameter (d_v), its volume can be expressed as $V = \frac{\pi}{6} d_h^2 d_v$ and thus:

$$d_{eq} = (d_h^2 d_v)^{1/3} \tag{11}$$

Furthermore, the ratio of the bubble deformation (E) was calculated as

$$E = \frac{d_h}{d_v} \tag{12}$$

For the capillary used in our experiments (d_c = 0.075 mm), the equivalent bubble diameter in pure water was 1.48 ± 0.02 mm, whereas for surfactant solutions, a detailed discussion of this parameter is provided in Section 3.2.2. Rising bubble velocity and deformation.

3. RESULTS AND DISCUSSION

3.1. Pure Water. As a first step in our study, we investigated the influence of *n*-hexane vapor on the pure water−air interface. For stationary interfaces, this problem has been extensively studied, though the outcomes are not always consistent. Mys et al.[18] used bubble pressure tensiometry with a specialized cell for generating saturated *n*-hexane vapor and measured dynamic surface tension over a time range of 0.01−30 s. Their results were compared with data from bubble profile analysis tensiometry. Notably, both methods showed no significant decrease in surface tension within approximately 1 min of interface formation. Nguyen et al.[12] employed bubble profile analysis tensiometry and found that perfluorohexane-saturated vapor reduced the surface tension of bubbles in water by about 4 mN/m. However, the kinetics of this process was not discussed. Our detailed experiments with *n*-hexane vapor revealed a similar scenario, which is discussed in the following sections.

Figure 3A presents results for the dynamic surface tension $\gamma(t)$ of bubbles with and without *n*-hexane vapor in pure water. When a '1st' bubble is formed in an experiment with *n*-hexane vapor, the initial surface tension is virtually the same as that for bubbles without *n*-hexane vapor ($\gamma_0^{W/A} \approx 72$ mN/m). The subsequent decrease in surface tension is attributed to the adsorption of *n*-hexane molecules from the gas phase, where

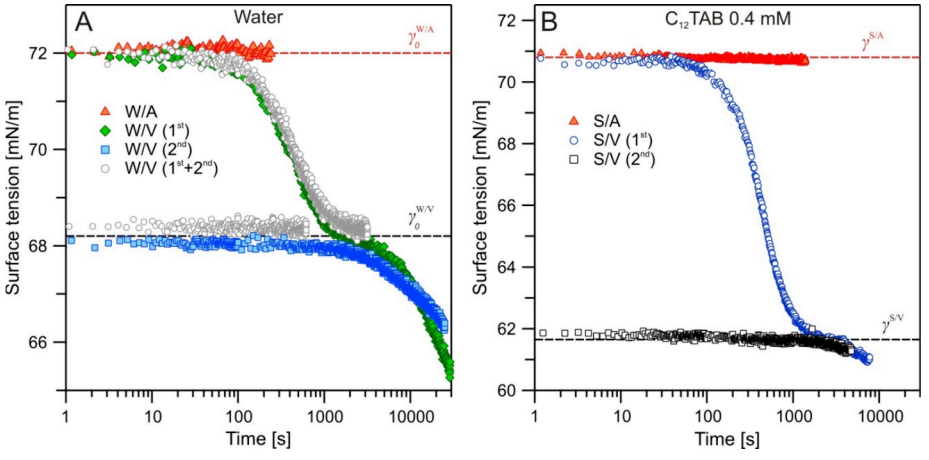

Figure 3. Dynamic surface tension measurements of stationary air bubbles in the absence or presence of *n*-hexane vapor; (1st) denotes the first bubble formed under unsaturated gas-phase conditions and (2nd) denotes the second bubble formed after vapor saturation (for details see in the text). (A) Pure water (W/A or W/V interface). (B) 0.4 mM C_{12}TAB solution (S/A or S/V interface).

https://doi.org/10.1021/acs.iecr.5c02608
Ind. Eng. Chem. Res. 2025, 64, 20347−20361

the partial vapor pressure P of *n*-hexane gradually increases over time up to the saturation pressure P_0. After approximately 20 min, the surface tension reaches a value of $\gamma \approx 68$ mN/m. The obtained $\gamma(t)$ curves resemble the adsorption kinetics behavior of amphiphile molecules adsorbing from solution. However, in this case, the gradual increase of the surface excess of *n*-hexane is determined by the gradual increase of P in the gas reservoir. When a '2nd' bubble is formed at P_0, the surface tension immediately stabilizes at $\gamma \approx 68$ mN/m and remains constant for at least half an hour. The same behavior of virtually instantaneous establishment of a steady-state surface tension was also observed in experiments with a pendant water drop grown in a presaturated *n*-hexane vapor atmosphere.[15] Furthermore, the steady-state surface tension values of $\gamma \approx 66-68$ mN/m (P_0 at 22−24 °C) obtained in those experiments,[15] together with data ($\gamma \approx 68$ mN/m, P_0 at 25 °C) measured by the methods of maximum bubble pressure and capillary rise are in very good agreement with our results.[7] Therefore, the surface tension value for the pure water/air interface in the presence of saturated *n*-hexane vapor ($P_0 \approx 19.3 \pm 0.8$ kPa at 24 ± 1 °C) was determined to be $\gamma_0^{W/V} = 68.3 \pm 0.3$ mN/m. For surfactant solutions, this value for $\gamma_0^{W/V}$ was used later on to recalculate the surface tension isotherms $\gamma(c_S)$ in terms of the surface pressure $\Pi(c_S)$.

The observed surface tension decrease of ≈ 4 mN/m in the presence of saturated *n*-hexane vapor is attributed to the formation of an adsorption layer of *n*-hexane molecules. This has been demonstrated by experiments with ellipsometry and neutron reflectometry for planar surfaces.[60,61] The latter study reported a surface excess value of about 0.6 μmol/m^2 for *n*-hexane on pure water measured at P_0 (at 25 °C), which is comparable to the P_0 used in the present study. The free energy of adsorption of *n*-hexane vapor on water in the "near-zero" coverage regime was reported to vary in the range of ca. 11−14 kJ/mol with temperature (0−25 °C).[10] Further information came from our MD simulation results (Figure 4), which revealed that *n*-hexane molecules, initially present in vapor form, began to accumulate at the water/gas interface.

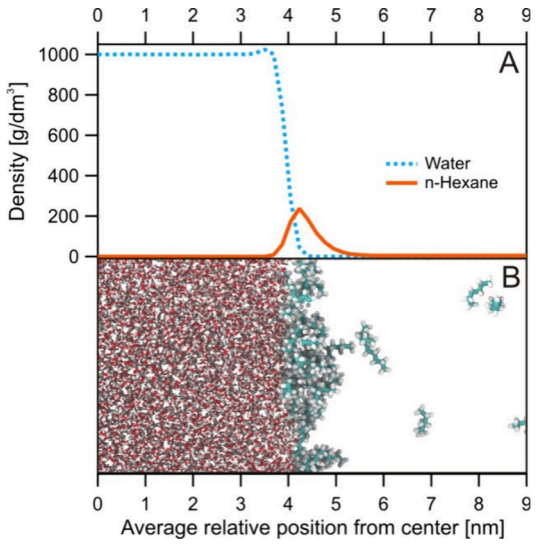

Figure 4. Molecular dynamics simulations of *n*-hexane adsorption from the vapor phase onto the pure water surface: (A) density profiles across the *z*-axis (perpendicular to the interface) and (B) visualization of the adsorption layer.

Interestingly, this layer does not reach an equilibrium thickness but continues to grow as molecules from the gas phase saturate it, forming a thin condensed *n*-hexane layer on the water/air interface. This phenomenon, observed in the MD simulations has been discussed by Hauxwell and Ottewill with formation of an organic thin liquid film between the water and the vapor phases,[8] which apparently leads to the observed further decrease in the interfacial tension below $\gamma_0^{W/V}$ at "long" times (see Figure 3). Very similar trend was observed in the time evolution of the ellipsometric signal in the experiments by Pfohl et al.[60] Together with Brewster angle microscopy observations, the ellipsometry results at "short" times (on the order of an hour) were interpreted as indicative for a "dilute" hexane monolayer (where gaseous and liquid expanded two-dimensional phases coexist). Apparently, such state is characterized by nearly constant surface tension (here defined as $\gamma_0^{W/V}$). At longer times, the monolayer evolves as a homogeneous liquid condensed phase and further to a multilayer structure topped with micrometric liquid hexane droplets.[60] For a pendant water drop, the accumulation of a condensed organic phase proceeds with the formation of an oil lens over the drop's apex area, which causes strong deviations from a Laplacian shape.[15] We believe that in the present case of a static buoyant bubble, accumulation of a liquid *n*-hexane phase presumably does not occur at the bubble's surface, because if any such liquid phase is formed it should leak down into the capillary that supports the bubble. This scenario is proved by the fact that we did not observe any deviations from a Laplacian shape for the bubbles under investigation and the standard deviation of the Laplace equation fitting to the experimental bubble profile of about 1 μm (typical for the drop/bubble shape analysis method) remained constant in all the experiments performed in this study (data not shown).[15] Hence, as discussed above, the observed decrease of the surface tension below $\gamma_0^{W/V}$ may be attributed to the formation of a thin liquid film of *n*-hexane, which does not have the properties of a bulk liquid phase. While there is no doubt that these phenomena require further investigation, they fall beyond the scope of this study and are therefore not discussed in detail here.

Focusing on the results of the rising bubble experiments, Figure 5A and B present comparisons of the variations of the bubble's local velocity and degree of the shape variations with distance from the capillary in water for clean air and air/*n*-hexane vapor systems. In both cases, the bubble velocity profiles consist of two stages, namely acceleration and terminal velocity. The terminal velocities were 35.2 ± 0.4 cm/s and 34.8 ± 0.3 cm/s for the W/A and W/V systems, respectively. Unlike the very recent literature report by Lotfi et al.,[35] which, to our best knowledge, is so far the only one dealing with rising bubbles of organic vapors, we were unable to clearly detect any effects of *n*-hexane vapor on the movement of an air bubble in pure water. Additional experiments performed with water conditioned with *n*-hexane (water shaken with liquid *n*-hexane in a flask and left to rest overnight prior to measurements) did not affect the rising velocity of air bubbles, whether *n*-hexane vapor was present or not.

Keeping in mind that variations in the hydrodynamic boundary conditions at a liquid/gas interface (retardation of the bubble surface fluidity) are caused by motion-induced surface tension gradients, this lack of observed effects on the bubble movement indicates deficiency of dynamic adsorption layer formation from *n*-hexane molecules, i.e., the bubble

https://doi.org/10.1021/acs.iecr.5c02608
Ind. Eng. Chem. Res. 2025, 64, 20347−20361

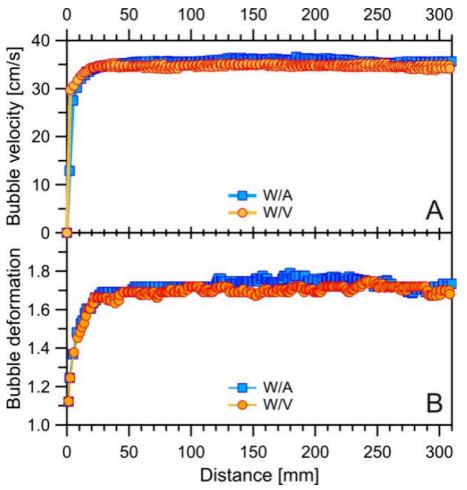

Figure 5. (A) Local velocity and (B) bubble deformation profiles as a function of distance from capillary for clean air (W/A interface) and air/*n*-hexane vapor (W/V interface) system in pure water (d_{eq} = 1.48 ± 0.02 mm).

surface remains fully mobile.[29] The fact that no effect on bubble velocity was detected is rather surprising, as bubble velocity typically shows greater sensitivity to changes in the water/air interface properties (such as adsorption layer formation) compared to surface tension measurements with a static W/A interface.[3] However, based on literature data,[62] it can be shown that a surface tension difference of the order of 4 mN/m has almost negligible influence on deformation (approximately 1%). Therefore, it can be hypothesized that the *n*-hexane layer at the pure water/air interface does not affect its fluidity. The physical background of this intriguing finding is unknown at the moment and further detailed experimental and theoretical investigations are needed to clarify it. At this stage, we can only speculate that the inability of *n*-hexane vapor molecules to generate surface tension gradients on the bubble surface arises from the dominance of aerodynamic forces, which exceed the free energy of adsorption of *n*-hexane at the water/air interface (ca. 11−14 kJ/mol in the "near-zero" coverage regime,[10] i.e., ∼5 kT). Molecular dynamics simulations further indicate negligible penetration of *n*-hexane into the aqueous phase, and the relatively small adsorption energy compared to the hydrodynamic drag on a rising bubble supports this interpretation. As a consequence, *n*-hexane molecules can readily desorb from the rear of the bubble, circulate within the gas phase, and readsorb at the top. This mechanism is additionally supported by the high diffusivity of *n*-hexane in air, which is several orders of magnitude greater than that of typical surfactants in water. Such rapid redistribution likely prevents the establishment of stable surface concentration gradients, which are usually responsible for stagnant cap formation in the case of surfactants adsorbing from the liquid phase.

3.2. Surfactant Solutions. *3.2.1. Stationary Bubble.* Literature data suggest that in the presence of surface active substances, the influence of organic vapor on the water/gas interface is much more pronounced than in pure water.[17−19] Thus, we performed a series of measurements using two surfactants: (i) the cationic one C_{12}TAB and (ii) the nonionic *n*-octanol.

Figure 3B presents results for the dynamic surface tension, $\gamma(t)$, of bubbles with and without *n*-hexane vapor in C_{12}TAB solution of c_S = 0.4 mM. Apparently, the presence of surfactant at this concentration has minimal effect on the surface tension of the S/A interface ($\Pi \approx 1$ mN/m), whereas in the case of the

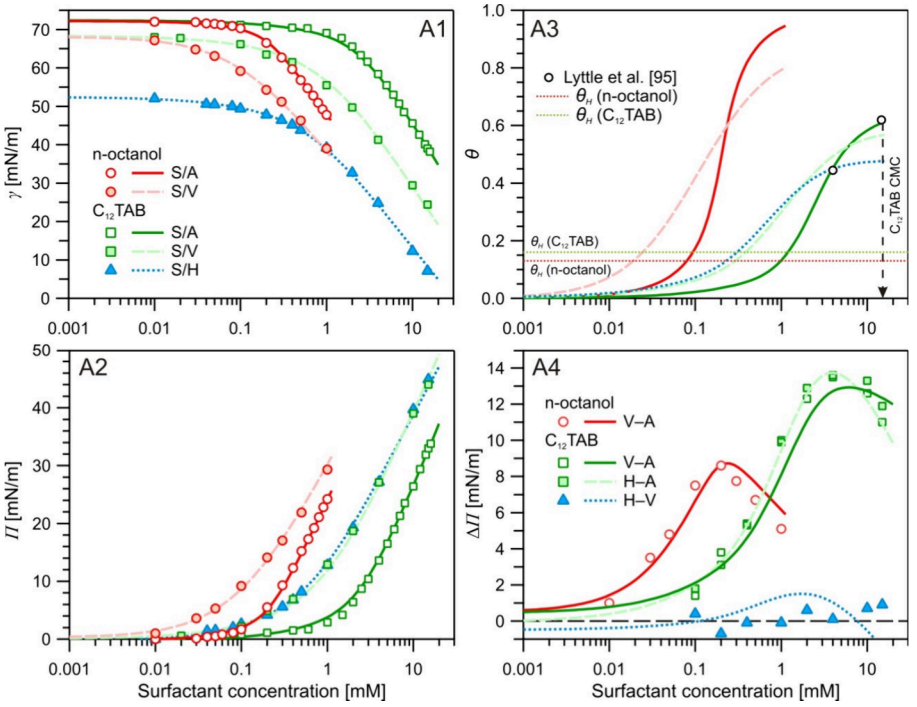

Figure 6. Surface tension data for *n*-octanol and C_{12}TAB solutions against air (S/A), *n*-hexane vapor (S/V), or liquid *n*-hexane (S/H); symbols represent experimental data, while lines indicate the best-fit of the STDE adsorption model: eq 1 for *n*-octanol and eqs 2−8 for C_{12}TAB. (A1) Surface tension isotherms $\gamma(c_S)$; (A2) corresponding surface pressure isotherms $\Pi(c_S)$; (A3) adsorption isotherms $\theta_S(c_S)$, dotted lines indicate θ_H for both S/V interfaces; (A4) dependences $\Delta\Pi(c_S)$ obtained from the data in (A2), for denotations and definitions, see eqs 13a−13c.

https://doi.org/10.1021/acs.iecr.5c02608
Ind. Eng. Chem. Res. 2025, 64, 20347−20361

S/V interface, the effect is much stronger ($\Pi \approx 6$ mN/m), which should be attributed to synergistic coadsorption of surfactant and *n*-hexane molecules at the interface. It is worth mentioning that, similar to the pure water system shown in Figure 3, the '1st' bubble required some time to reach a constant surface tension value of $\gamma \approx 62$ mN/m, while for the '2nd' bubble, this value was established immediately after its formation.

Figure 6-A1 presents the experimental and theoretical surface tension $\gamma(c_S)$ isotherms for both surfactants at the different interfaces studied. For illustrative purposes, Figure 6-A2 presents these data in terms of the corresponding $\Pi(c_S)$ isotherms. The evaluated theoretical adsorption isotherms $\Gamma(c_S)$ are presented in Figure 6-A3 in the form of dimensionless surface coverage, $\theta = \Gamma(c_S)/\Gamma_{S\infty}$, which provides a more meaningful basis for comparison between the studied systems. For reference, experimental data from the literature were also included.[63] It should be emphasized that for fitting the isotherms at the S/V interface, the parameter $\Gamma_{S\infty}$ was kept fixed at the value obtained from the best fit of the isotherm at the S/A interface, as it is determined by the size of the hydrophilic headgroup of the surfactant. The parameter values used for the best fit of each data set are listed in Table 1.

Table 1. Best-Fit Parameters of STDE Adsorption Models: eq 1 for *n*-Octanol and eqs 2−8 for C_{12}TAB

Interface	α_S [mol/m^3]	$\Gamma_{S\infty}$ [mol/m^2]	H_S	θ_H	χ^2 [(mN/m)^2]
		n-octanol			
S/A	7.5×10^{-1}	6.0×10^{-6}	3.2	0.00	0.10
S/V	1.1×10^{-1}	6.0×10^{-6}	0.0	0.13	0.17
		C_{12}TAB[a]			
S/A	3.5×10^{-2}	5.6×10^{-6}	6.2	0.00	0.27
S/V	5.0×10^{-4}	5.6×10^{-6}	0.0	0.16	0.54
S/H	4.0×10^{-4}	5.6×10^{-6}	0.0	0.18	0.12

[a]Additional STDE model parameters for C_{12}TAB, i.e., $\alpha_c = 2.8 \times 10^6$ mol/m^3, $g_{CS} = 0.64$, $\delta = 0.34$ nm, and $\varepsilon_{St} = 26$, were taken from work of Para et al.[38]

As mentioned above, in the present analysis, the so-called blocking parameter θ_H was set constant. This parameter reflects the fraction of the total surface area occupied by adsorbed *n*-hexane molecules, and thus, it is unavailable for surfactant adsorption. In reality, the *n*-hexane partial surface coverage is indeed dependent on the partial surface coverage by other molecules (here denoted θ_S) at the interface, e.g., either spread insoluble molecules at different surface concentrations or soluble surfactants adsorbed from solutions with various bulk concentrations.[19] However, the theoretical estimations (based on experimental surface tension data) in those studies, as well as direct neutron reflectometry measurements,[61] revealed that the effect of the surface concentration of other molecules on θ_H of *n*-hexane is relatively weak.

Analyzing the best-fit parameter values (Table 1) reveals that, for both surfactants, the values of the 'surface activity' parameters, α_S, for the S/A interface increased with introduction of *n*-hexane vapor (S/V interface) and the corresponding increase of free energy of adsorption can be evaluated as $kT \ln \frac{\alpha_S^{S/A}}{\alpha_S^{S/V}} = 4.8$ kJ/mol for *n*-octanol and $kT \ln \frac{\alpha_S^{S/A}}{\alpha_S^{S/V}} = 17.8$ kJ/molfor C_{12}TAB. Such an increase in the adsorption free energy can be predominantly attributed to the van der Waals interactions between surfactants' hydrocarbon chains and adsorbed hexane molecules. On the other hand, interactions between surfactant chains are screened by the presence of *n*-hexane molecules, which impose conformational restrictions on adsorption, thereby $H_S = 0$. For C_{12}TAB, the free energy of adsorption increases by $kT \ln \frac{\alpha_S^{S/A}}{\alpha_S^{S/H}} = 18.8$ kJ/mol when air (S/A interface) is replaced by liquid *n*-hexane (S/H interface). Apparently, the free energy of C_{12}TAB adsorption at the S/H interface is not significantly higher than that at the S/V interface. This finding is well illustrated by the overlapping surface pressure isotherms for the S/H and S/V interfaces shown in Figure 6-A2. This suggests the thin liquid film of adsorbed *n*-hexane is capable of imposing the same intermolecular interactions at the interface as in the case of a bulk liquid *n*-hexane phase.

The effect of the nature of the interface on the surfactant adsorption energy can be conveniently illustrated by visualizing the surface tension or surface pressure shifts in the isotherms for the S/V (or S/H) interface relative to the corresponding values for the S/A interface, taken as the reference. The surface pressure shift is defined as

$$\Delta\Pi^{V-A}(c_{S,i}) = \Pi^{S/V}(c_{S,i}) - \Pi^{S/A}(c_{S,i}) \quad (13a)$$

$$\Delta\Pi^{H-A}(c_{S,i}) = \Pi^{S/H}(c_{S,i}) - \Pi^{S/A}(c_{S,i}) \quad (13b)$$

$$\Delta\Pi^{H-V}(c_{S,i}) = \Pi^{S/H}(c_{S,i}) - \Pi^{S/V}(c_{S,i}) \quad (13c)$$

The obtained experimental and theoretical dependences $\Delta\Pi(c_S)$ are presented in Figure 6-A4.

The same approach was already used by other authors in experiments with the systems C_{12}TAB solution/*n*-hexane vapor and dioctanoylphosphatidylcholine solution/perfluorohexane vapor.[12,16] In the latter study, the authors found that $\Delta\Pi^{V\text{-}A}$ increased linearly with the logarithm of the lipid concentration c_S. In contrast, our results for both surfactants revealed nonmonotonic dependences with a maximum of about $\Delta\Pi^{V\text{-}A} \approx 9$ mN/m for *n*-octanol and $\Delta\Pi^{V\text{-}A} \approx 14$ mN/m for C_{12}TAB, emerging at intermediate surfactant concentrations. Notably, our data for C_{12}TAB are in good agreement with those by Javadi et al.[16] for an equivalent system probed by the pendant drop technique (maximum at $\Delta\Pi^{V\text{-}A} \approx 16$ mN/m). This shows that at lower surfactant surface coverages, where spatial obstacles and intermolecular interactions between surfactant molecules are relatively weak, the free energy of transfer of hydrocarbon chain from water into *n*-hexane layer is higher than into air as the desorption of surfactant molecules is likely reduced by the presence of *n*-hexane molecules at the S/V interface. That is reflected in the magnitude of α_S parameter, and leads to greater surface coverage compared to the hexane-free system. However, at high surfactant concentrations, the surfactant monolayer becomes densely packed, and the situation changes significantly. Here, the presence of *n*-hexane molecules hinders surfactant adsorption due to geometrical and conformational constraints, resulting in lower surfactant coverage compared to the hexane-free surface (Figure 6-A3). Hence, one may distinguish between two distinct effects in the interactions of surfactant and *n*-hexane molecules at the S/V interface − synergism (low c_S) and blocking effect (high c_S), which appear relevant for both types of surfactants investigated in the

https://doi.org/10.1021/acs.iecr.5c02608
Ind. Eng. Chem. Res. 2025, 64, 20347−20361

present work. A similar concept was discussed by Campbell at al.[61] in their neutron reflectometry study. These two effects are responsible for the observed maximum in the $\Delta\Pi^{V\text{-}A}(c_S)$ dependencies in Figure 6-A4, which virtually coincide with the crossover of the respective adsorption isotherms $\Gamma^{S/A}(c_S)$ and $\Gamma^{S/V}(c_S)$ in Figure 6-A3. Recalling our assumption that the surface coverage of *n*-hexane θ_H is taken constant and independent of the surfactant surface concentration, it should be mentioned that more detailed analysis might be achieved by employing θ_H as an adjustable parameter in the fitting procedure. This, in turn, would alter the position of the crossover between the $\Gamma^{S/A}(c_S)$ and $\Gamma^{S/V}(c_S)$ isotherms, as well as the extent of the shift of $\Gamma^{S/V}$ from $\Gamma^{S/A}$ (Figure 6-A3). Note that the discussed crossover was also observed in previous theoretical works that have accounted for variation in θ_H.[19]

The more pronounced maximum in the $\Delta\Pi^{V\text{-}A}(c_S)$ dependence for C_{12}TAB compared to the one for *n*-octanol implies that *n*-hexane molecules interact stronger with longer alkyl chains. Moreover, the overlap of the $\Delta\Pi^{S/V}(c_S)$ and $\Delta\Pi^{S/H}(c_S)$ isotherms, resulting in a weak $\Delta\Pi^{H-V}$ dependence, provide further evidence that a thin *n*-hexane film was formed on the water/air interface. Such thin liquid film makes the bubble surface identical to the *n*-hexane drop surface in terms of the adsorption process of surfactant.[8]

Molecular dynamics simulations provide further insight into adsorption and desorption processes of surfactants depending on the presence of *n*-hexane. Figure 7 illustrates differences in

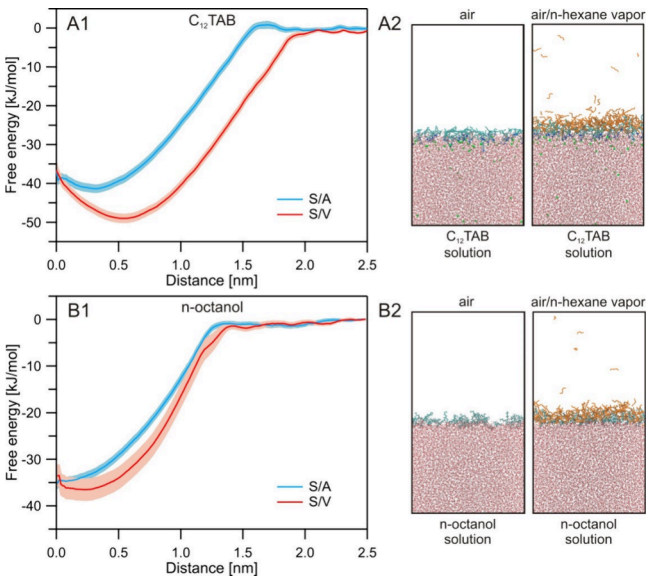

Figure 7. (A1, B1) Free energy profiles for surfactant molecule removal from the interface. (A2, B2) Visualizations of the adsorption layer for S/A and S/V interfaces for C_{12}TAB (A1) and (A2) and *n*-octanol (B1) and (B2). *n*-Hexane molecules are highlighted in orange.

the desorption free energy of a surfactant molecule. The displacement of the molecule from the interface into the bulk water requires more energy when the interface is enriched with *n*-hexane molecules compared to hexane-free surfaces for both studied surfactants. This effect is more pronounced for C_{12}TAB, due to the longer hydrocarbon chain compared to *n*-octanol, leading to stronger van der Waals interactions between *n*-hexane and C_{12} alkyl chains, and the differences are in good agreement with the ones for the free energy of adsorption calculated using model isotherms. The MD simulations provide a molecular-level explanation of the experimental outcome observed in Figure 6-A4, where the maximum in the $\Delta\Pi^{V\text{-}A}(c_S)$ dependencies is more pronounced for C_{12}TAB. Hindrance of the surfactant desorption process by *n*-hexane is the origin of the described above synergistic effect, which leads to the greater surfactant surface excess at the S/V interface observed for a given bulk concentration, and this situation is illustrated by the MD simulations presented in Figure 7, where the surfactant surface excess was set at $\Gamma_S = 1.3$ μmol/m^2.

3.2.2. Rising Bubble Velocity and Deformation. The pronounced effect of *n*-hexane vapor on the stationary water/gas interface provided a reason for conducting measurements on a nonstationary water/gas interface. Therefore, a series of rising bubble experiments was performed in solutions of C_{12}TAB and *n*-octanol, respectively.

It was found that, unlike in pure water, the presence of *n*-hexane vapor inside a rising bubble in a surfactant solution significantly impacts its movement. Figure 8 presents bubble velocities and deformations in solutions of both surfactants at concentrations where the differences in bubble dynamics between the S/A and S/V systems were most pronounced. For the air/*n*-hexane system, we observed a decrease in bubble maximum velocity, terminal velocity, and deformation. Moreover, in the concentration ranges where the deceleration stage occurred, a reduction in the distance required to reach terminal velocity was noted (see Figure 8-B1). The data in Figure 8 clearly indicate that the formation of the dynamic adsorption layer (DAL), which eventually leads to bubble surface immobilization, occurs more rapidly in the presence of *n*-hexane vapor inside the bubble. This occurs despite the fact that *n*-hexane molecules themselves do not directly affect the fluidity of the liquid/gas interface (see data for pure water in Figure 5A). This suggests that a synergistic interaction between *n*-hexane and surfactant molecules may be responsible for altering the kinetics of DAL formation, ultimately modifying the hydrodynamic drag.

Figure 9A presents data on the terminal velocity of bubbles as a function of surfactant concentration. To quantify the effect of *n*-hexane vapor inside the bubble, the experimental data were analyzed using the equation proposed by Kowalczuk et al.:[64]

$$U = U_{min} + (U_{max} - U_{min}) \cdot e^{-3(c_S/CMV)^2} \quad (14)$$

where U_{min} and U_{max} are the minimum and maximum terminal velocities, respectively and *CMV* (concentration at minimum velocity) is the surfactant concentration required to reach minimum velocity, i.e., *CMV* indicates the conditions required for fully immobilizing the bubble surface fluidity. In our considerations, we assume that minor variations of the gas density in the investigated bubbles due to the presence of *n*-hexane vapor have a negligible effect on the bubble buoyancy.[12]

For our experiments, values of the minimum and maximum terminal velocities are well-known: U_{max} is the terminal velocity observed in pure water (≈ 35 cm/s), while U_{min} was measured to be 14.8 cm/s, which is in good agreement with literature data for the same bubble diameter.[3] The *CMV* values for the studied systems were fitted using Eq. 14, and the best fit results are presented in Table 2. For clean air systems, the *CMV* values showed very good agreement with the literature data.[64]

https://doi.org/10.1021/acs.iecr.5c02608
Ind. Eng. Chem. Res. 2025, 64, 20347−20361

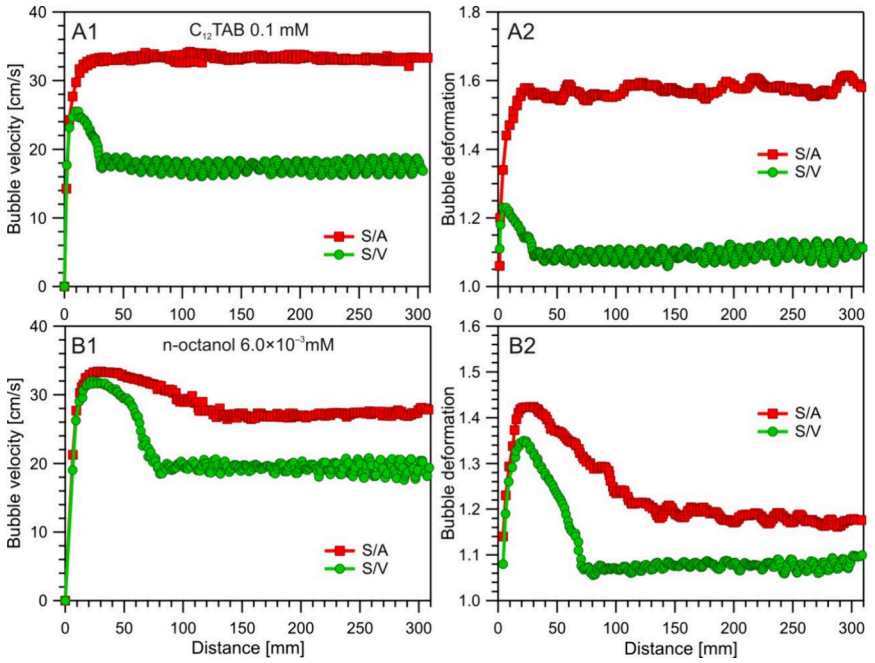

Figure 8. Bubble local velocity (A1) and bubble deformation (A2) for 0.1 mM C_{12}TAB; bubble local velocity (B1) and bubble deformation (B2) for 6.0 × 10^{-3} mM *n*-octanol.

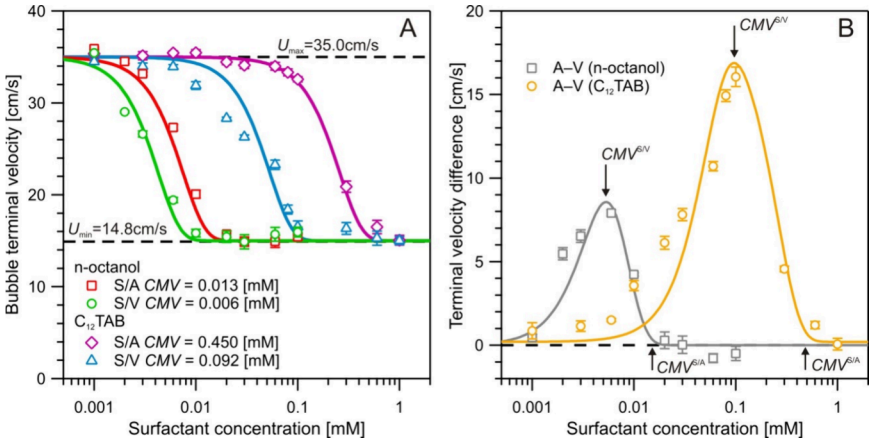

Figure 9. (A) Bubble terminal velocity and (B) terminal velocity difference as a function of surfactant concentration in the absence (S/A interface) or presence (S/V interface) of *n*-hexane vapor. The lines are theoretical curves obtained using eqs 14 and 15, respectively.

Table 2. Concentrations at Minimum Veloci0ty (*CMV*) for Studied Systems

	CMV [mM]	
	C_{12}TAB	*n*-octanol
S/A	0.450	0.013
S/V	0.092	0.006

Moreover, the effect of *n*-hexane presence on the dynamic adsorption layer over the rising bubble could be illustrated by visualizing shifts in the bubble's terminal velocity, defined as

$$\Delta U^{A-V}(c_{S,i}) = U^{S/A}(c_{S,i}) - U^{S/V}(c_{S,i}) \quad (15)$$

Reaching the minimum velocity by the bubble means that further increase of the surfactant concentration has no influence on the bubble terminal velocity. In other words, the coverage of the bubble interface becomes sufficient to fully immobilize the bubble surface. Therefore, the observed decrease in the *CMV* values may indicate that, at the same c_S, surfactant coverage over the rising bubble surface is significantly greater in the presence of *n*-hexane vapor. Regardless of the type of surfactant used, the bubble terminal velocity is always lower in the air/*n*-hexane vapor system than in the clean air system, but the magnitude of this effect varies with the type of surfactant (see Figure 10B) and its c_S. Similarly to the $\Delta\Pi^{V\text{-}A}(c_S)$ dependence (see Figure 6-A4), a maximum in the $\Delta U^{A\text{-}V}(c_S)$ dependence is observed.

The initial increase in $\Delta U^{A\text{-}V}(c_S)$ is associated with greater surfactant coverage on the bubble surface in the air/*n*-hexane vapor system, leading to a significant reduction in the bubble's terminal velocity. It worth mentioning that the maximum $\Delta U^{A\text{-}V}$ is observed at the $CMV^{S/V}$ value. Further increasing the surfactant concentration beyond the *CMV* value determined in the hexane-free system reduces $\Delta U^{A\text{-}V}$ to zero, as full immobilization of the bubble surface is achieved (bubble terminal velocity is U_{min} = 14.8 cm/s) in both studied systems.

https://doi.org/10.1021/acs.iecr.5c02608
Ind. Eng. Chem. Res. 2025, 64, 20347−20361

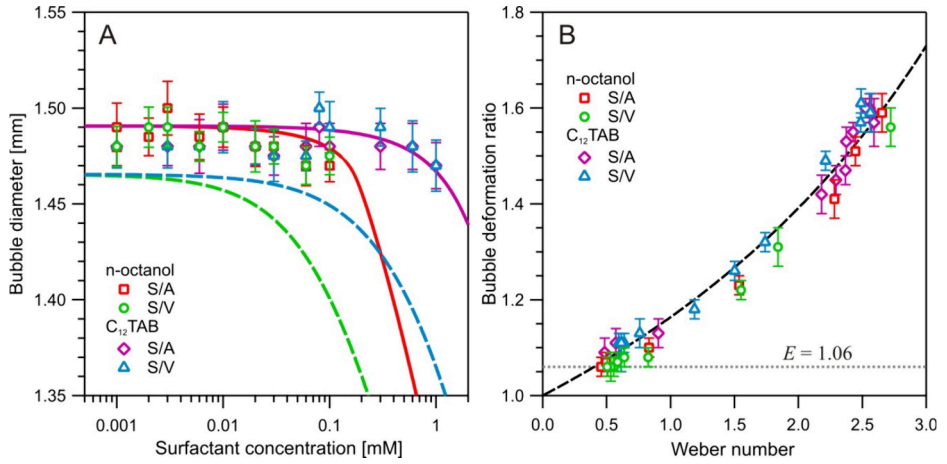

Figure 10. (A) Bubble diameter as a function of surfactant concentration and (B) bubble deformation ratio as a function of the Weber number in the absence (S/A interface) or presence (S/V interface) of *n*-hexane vapor. The lines are theoretical curves obtained using eqs 16 and 17, 18, respectively.

Based on the presented data it is observed that (i) the *CMV* decrease is greater in case of C_{12}TAB (Table 2) and (ii) the terminal velocity difference is more pronounced, again, for C_{12}TAB (Figure 9B). These findings correlate well with surface tension measurements and MD simulations, which also demonstrated a stronger synergistic effect of *n*-hexane vapor and surfactant for C_{12}TAB compared to *n*-octanol.

When collecting experimental data on bubble velocity, it is crucial to measure the bubble diameter for each experiment, as changes in bubble volume significantly impact the buoyant force. Therefore, the bubble equivalent diameter should be carefully estimated using eq 2, with d_v and d_h obtained from image analysis. Additionally, theoretical bubble diameter values can be predicted using Tate's law:[65]

$$d_b = \left(\frac{6 d_c \gamma}{\Delta\rho g}\right)^{1/3} \tag{16}$$

where d_c is the capillary inner diameter, $\Delta\rho$ is the density difference between water and the gas used, and g is the gravitational acceleration.

Both, experimental and theoretical values of bubble diameter as a function of surfactant concentration, are shown in Figure 10A. As it is seen, the theoretical values of bubble diameter show good consistency with experimental data for the hexane-free air bubble, while theoretical data for the air/*n*-hexane vapor systems (dashed lines) underestimate bubble diameter. It means that for the air/*n*-hexane vapor system, the process of the bubble growth on the capillary tip is not influenced by the presence of organic vapors. Without any doubt, the increase in gas density due to *n*-hexane vapor presence is not great enough to compensate for the decrease of surface tension. On the contrary, even a small increase of the effective capillary inner diameter (ca. 5 μm, i.e., 7%) caused by condensation of *n*-hexane on the capillary tip may lead to an observed increase of bubble size for clean water and low surfactant concentrations. However, this hypothesis fails for higher surfactant concentrations: for 0.1 mM C_{12}TAB, surface tensions are 69.1 and 55.5 mN/m for S/A and S/V interfaces, respectively. To compensate for this surface tension difference and obtain the same bubble diameter, the effective capillary inner diameter needs to increase by ca. 20 μm (i.e., 25%). While small changes (up to 5 μm) of the effective capillary inner diameter might be hard to observe with the optical lens used in our setup, the 20 μm increase of the bubble neck size can be easily recognized from image analysis. Therefore, this explanation should be rather rejected. Another possible explanation of this surprising effect might be related to the time of bubble formation on the capillary tip before it detaches and starts rising to the top of the column. In our case, the time of bubble formation is in the range 1.5−2 s, and this time scale might be too short for the immediate formation of the *n*-hexane layer over the bubble interface.

A thorough interpretation of this intriguing issue requires further studies for a quantitative description of the phenomenon, particularly through dynamic surface tension measurements and bubble LVP measurements under controlled bubble growth and detachment conditions.

Besides bubble velocity, changes in bubble motion are always reflected in another characteristic quantity, i.e., bubble deformation ratio (E). It is clearly observed for surfactant solutions that a decrease in the bubble velocity is followed by a decrease in the bubble deformation ratio. Legendre et al.[66] proposed a simple formula describing the bubble deformation in pure water for $E < 3$:

$$E = \left(1 - \frac{9}{64} We\right)^{-1} \tag{17}$$

where We is the Weber number:

$$We = \frac{d_b U_b^2 \Delta\rho}{\gamma} \tag{18}$$

Figure 10B presents a comparison between experimental data and theoretical values calculated using eqs 17−18 for bubble deformation ratio at the terminal velocity as a function of the Weber number. Regardless of the limitations of eq 17 for pure water only,[66] the theoretical model follows the experimental results quite well up to the concentrations at minimum velocity. Above the *CMV* (corresponding to a low Weber number value in our system), bubble deformation tends to a constant value of $E \approx 1.06$. Under these conditions, the theoretical model may deviate from the experimental data, primarily because the bubble's terminal velocity reaches its minimum and remains constant despite increasing surfactant concentration, while surface tension continues to decrease. It is

https://doi.org/10.1021/acs.iecr.5c02608
Ind. Eng. Chem. Res. 2025, 64, 20347−20361

worth mentioning that there is no significant difference in bubble shape deformation between a pure air bubble and an air/*n*-hexane vapor bubble at the same terminal velocity. This may confirm that the adsorbed *n*-hexane layer does not influence the fluidity of the rising bubble.

3.2.3. Drag Coefficient and Reynolds Number Dependence. When a bubble reaches terminal velocity, its motion is driven by the balance between the buoyancy and the drag force. As the bubble size stayed almost constant (ca. 1.48 mm) for the studied concentration ranges, changes in the buoyant force are negligible. Thus, the decrease of the bubble terminal velocity as a function of the surfactant concentration is reflected in changes of the drag coefficient (C_D). Based on the experimental data, the drag coefficient can be found from[29]

$$C_D = \frac{4d_b\Delta\rho g}{3U_b^2\rho_L} \approx \frac{53200}{\mathrm{Re}^2} \tag{19}$$

$$\mathrm{Re} = \frac{d_b U_b \rho_L}{\eta_L} \tag{20}$$

where *Re* is the Reynolds number and η_L is the water viscosity.

Figure 11 presents the calculated drag coefficient values for experimental data using eq 19 as a function of the Reynolds number. As shown, the experimental data lie between the two theoretical curves representing the boundary conditions of fully mobile and tangentially immobile interfaces.

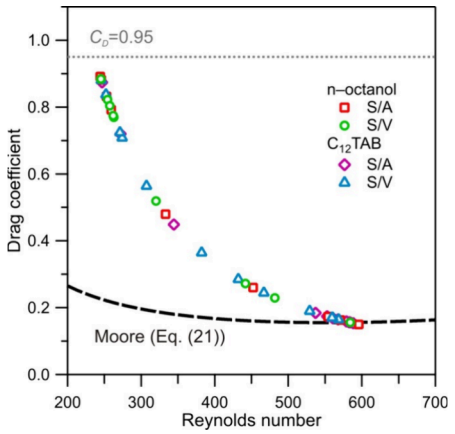

Figure 11. Drag coefficient as a function of Reynolds number; symbols present C_D values calculated using experimental data and eqs 19 and 20.

For mobile interface, which corresponds to pure water and very low surfactant concentrations and, consequently, high terminal velocities and high Reynolds numbers, the experimentally determined drag coefficients align well with the theoretical relation proposed by Moore:[67]

$$C_D = \frac{48}{\mathrm{Re}} G(E)\left[1 + \frac{2.21H(E)}{\sqrt{\mathrm{Re}}}\right] \tag{21}$$

where $G(E)$ and $H(E)$ are functions of the bubble deformation degree:[68]

$$G(E) = \frac{1}{3}E^{4/3}(E^2-1)^{3/2}\frac{\sqrt{E^2-1} - (2-E^2)\sec^{-1}E}{(E^2\sec^{-1}E - \sqrt{E^2-1})^2} \tag{22}$$

$$H(E) = 0.0195E^4 - 0.2134E^3 + 1.7026E - 1.5732 \tag{23}$$

On the other hand, for a fully immobile bubble surface and $Re > 130$, a drag coefficient of 0.95 has been proposed by Nguyen.[69] As shown, the experimental C_D values determined for high-concentration surfactant solutions approach this limiting value.

Across the entire Reynolds number range, no deviations are observed for air/*n*-hexane vapor systems. This consistency may indicate that the same mechanism − surface bubble immobilization by a dynamic adsorption layer − causes the terminal velocity decrease for both studied systems. An analysis of the bubble velocity profiles in pure water indicates that *n*-hexane vapor alone does not immobilize the bubble surface. Therefore, in both systems, it is the surfactant adsorption that is responsible for altering the bubble surface fluidity. Since the adsorption flux at the same surfactant concentration is similar regardless of the presence or absence of *n*-hexane vapor in the gaseous phase, the observed differences in surface coverage are most likely due to changes in the desorption process. Hindrances in the desorption process can effectively influence surfactant coverage on the rising bubble interface, causing a significant decrease in bubble velocity. Similar conclusions were drawn in the theoretical paper by Wang et al.,[70] dealing with effects of adsorption, desorption and diffusion characteristics of surfactants on the hydrodynamic characteristics of a bubble in a surfactant solution at medium Reynolds numbers. It was shown that an increase in Langmuir number (La) defined as

$$La = \frac{k_a \cdot c_S}{k_d} \tag{24}$$

where k_a and k_d are adsorption and desorption rate constants, respectively, either by an increase of k_a (as well as c_S) and/or a decrease of k_d, leads to an increase in the stagnant cap angle (β) and interfacial concentration, and consequently, a decrease in the bubble velocity. This mechanism is schematically presented in Figure 12.

4. CONCLUSIONS

The influence of organic vapor on the physicochemical properties of water/air interface has long been debated, as overviewed in the introduction, but only a few studies have

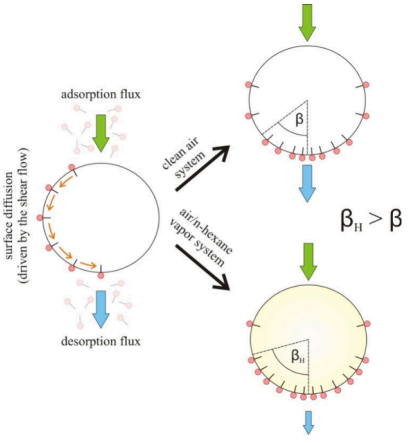

Figure 12. Schematic view of the immobilization mechanism in the presence of *n*-hexane vapor.

https://doi.org/10.1021/acs.iecr.5c02608
Ind. Eng. Chem. Res. 2025, 64, 20347−20361

examined directly dynamic adsorption layer formed over the rising bubble.[35] In our study, the influence of *n*-hexane vapor on rising bubbles in pure water and in surfactant solutions of *n*-octanol or C_{12}TAB was thoroughly examined and interpreted based on supporting interfacial tension measurements and molecular dynamics simulations.

It was found that the presence of *n*-hexane vapor significantly influences surface tension, even in pure water systems. A thorough analysis of the obtained data using the STDE isotherm revealed two major adsorption regimes. In the first regime, which includes low and medium surfactant concentrations, cooperative adsorption of surfactant and *n*-hexane molecules was observed, leading to a distinct increase in surface coverage compared to the hexane-free system. The second regime began at the surfactant concentration corresponding to the crossover point of surface coverages. Beyond this concentration, the surface coverage in the air/*n*-hexane system was lower than in the hexane-free system. This effect was attributed to hindered surfactant adsorption caused by geometrical and conformational constraints.

In the case of rising bubble experiments, no effect of *n*-hexane vapor was detected in pure water, whereas its presence significantly influenced bubble velocity profiles in surfactant solutions. This suggests that surfactant molecules adsorbed at the bubble interface play a crucial role in altering bubble mobility, and that the synergistic effect of surfactant and *n*-hexane molecules is essential for reducing the bubble's terminal velocity. It should be emphasized that the observed crossovers in surface coverage did not affect the bubble rise velocity, as the measured concentrations at minimum velocity (*CMV*) remained well below the crossover concentrations.

Measurements of both static and dynamic bubbles support the conclusion that the primary cause of the observed differences in bubble terminal velocities at water/air and water/vapor interfaces − under identical surfactant concentrations − was the higher surfactant coverage at the bubble interface in the presence of *n*-hexane vapor. Since the adsorption flux remains constant at a given surfactant concentration regardless of the presence of *n*-hexane vapor in the gas phase, the differences in surface coverages were likely due to changes in the desorption process. This finding has been confirmed by all-atom molecular dynamics simulations, which revealed that the presence of *n*-hexane in the interfacial layer hinders the desorption of surfactant molecules.

The presented results clearly demonstrate a significant influence of organic vapors on the enhancement of adsorption layer formation kinetics. This finding serves as a valuable starting point for further investigations into bubble dynamics, the formation of individual foam films, and the behavior of complete foam systems, all of which hold significant potential for a wide range of chemical engineering applications. Systematic investigations involving a diverse range of volatile compounds (e.g., natural) could pave the way for the design of multicomponent systems in which foam film stability and foaming efficiency are preserved − even when the concentration of surface-active agents is substantially reduced. Such an approach holds promising applications in industries such as cosmetics and pharmaceuticals, where the formulation of stable foams is essential. Moreover, this phenomenon can be strategically exploited in separation technologies that operate at gas/liquid interfaces, for instance foam fractionation for protein recovery or froth flotation in mineral processing. In these applications, the controlled presence of organic vapors within bubbles could significantly enhance recovery rates and enable a marked reduction in the amount of frothers required. Minimizing the use of synthetic surfactants without compromising process efficiency brings notable economic and environmental advantages. It also facilitates a transition toward greener alternatives, such as biosurfactants − biodegradable and less toxic substances that, despite their many benefits, remain prohibitively expensive for widespread adoption. In our opinion, the results presented in this paper provide a strong starting point for the development of a new generation of foam-based technologies that combine high performance with the principles of green chemistry and sustainable engineering.

AUTHOR INFORMATION

Corresponding Author

Dominik Kosior − *Jerzy Haber Institute of Catalysis and Surface Chemistry, Polish Academy of Sciences, 30-239 Krakow, Poland;* orcid.org/0000-0001-9549-4688; Email: Dominik.Kosior@ikifp.edu.pl

Authors

Georgi Gochev − *Jerzy Haber Institute of Catalysis and Surface Chemistry, Polish Academy of Sciences, 30-239 Krakow, Poland; Institute of Physical Chemistry, Bulgarian Academy of Sciences, 1113 Sofia, Bulgaria;* orcid.org/0000-0001-5033-3194

Piotr Batys − *Jerzy Haber Institute of Catalysis and Surface Chemistry, Polish Academy of Sciences, 30-239 Krakow, Poland;* orcid.org/0000-0002-2264-3053

Łukasz Witkowski − *Jerzy Haber Institute of Catalysis and Surface Chemistry, Polish Academy of Sciences, 30-239 Krakow, Poland*

Klaudia W. Zaręba − *Jerzy Haber Institute of Catalysis and Surface Chemistry, Polish Academy of Sciences, 30-239 Krakow, Poland*

Piotr Warszyński − *Jerzy Haber Institute of Catalysis and Surface Chemistry, Polish Academy of Sciences, 30-239 Krakow, Poland*

Jan Zawala − *Jerzy Haber Institute of Catalysis and Surface Chemistry, Polish Academy of Sciences, 30-239 Krakow, Poland;* orcid.org/0000-0003-4542-2226

Complete contact information is available at: https://pubs.acs.org/10.1021/acs.iecr.5c02608

Notes

The authors declare no competing financial interest.

ACKNOWLEDGMENTS

Partial financial support from the Polish National Science Centre (NCN, grant no. 2021/43/B/ST8/00053) is gratefully acknowledged. This work was also funded by the statutory funding of the Jerzy Haber Institute of Catalysis and Surface Chemistry, PAS. We gratefully acknowledge the Polish high-performance computing infrastructure PLGrid (HPC Center: ACK Cyfronet AGH) for providing computer facilities and support within the computational grant no. PLG/2024/017771.

REFERENCES

(1) Temesgen, T.; Bui, T. T.; Han, M.; Kim, T.; Park, H. Micro and Nanobubble Technologies as a New Horizon for Water-Treatment Techniques: A Review. *Adv. Colloid Interface Sci.* **2017**, *246*, 40−51.

(2) Sochacki, M.; Michorczyk, P.; Vogt, O. Foam Fractionation as an Efficient Method for the Separation and Recovery of Surfactants and Surface-Inactive Agents: State of the Art. *ACS Omega* **2025**, *10*, 55.
(3) Krzan, M.; Zawala, J.; Malysa, K. Development of Steady State Adsorption Distribution over Interface of a Bubble Rising in Solutions of N-Alkanols (C5, C8) and n-Alkyltrimethylammonium Bromides (C8, C12, C16). *Colloids Surf. A Physicochem. Eng. Asp.* **2007**, *298*, 42−51.
(4) Zawala, J.; Kosior, D.; Malysa, K. Formation and Influence of the Dynamic Adsorption Layer on Kinetics of the Rising Bubble Collisions with Solution/Gas and Solution/Solid Interfaces. *Adv. Colloid Interface Sci.* **2015**, *222*, 765−778.
(5) Vakarelski, I. U.; Yang, F.; Tian, Y. S.; Li, E. Q.; Chan, D. Y. C.; Thoroddsen, S. T. Mobile-Surface Bubbles and Droplets Coalesce Faster but Bounce Stronger. *Science Adv.* **2019**, *5* (10), No. eaaw4292.
(6) *Surfactants: Chemistry, Interfacial Properties, Applications*; Möbius, D., Miller, R., Fainerman, V. B., Eds.; Studies In Interface Science; Elsevier, 2001.
(7) Cutting, C. L.; Jones, D. C. Adsorption of Insoluble Vapours on Water Surfaces. Part I. *J. Chem. Soc.* **1955**, No. 0, 4067−4075.
(8) Hauxwell, F.; Ottewill, R. H. A Study of the Surface of Water by Hydrocarbon Adsorption. *J. Colloid Interface Sci.* **1970**, *34* (4), 473−479.
(9) Jho, C.; Nealon, D.; Shogbola, S.; King, A. D. Effect of Pressure on the Surface Tension of Water: Adsorption of Hydrocarbon Gases and Carbon Dioxide on Water at Temperatures between 0 and 50°C. *J. Colloid Interface Sci.* **1978**, *65* (1), 141−154.
(10) Hauxwell, F.; Pallas, N. R.; Pethica, B. A. Adsorption of N-Alkane Vapors on Water. *Langmuir* **1992**, *8* (2), 602−603.
(11) Lou, A.; Pethica, B. A. Adsorption of Hexane at the Water/Vapor Interface. *Langmuir* **1997**, *13* (19), 4933−4934.
(12) Nguyen, P. N.; Trinh Dang, T. T.; Waton, G.; Vandamme, T.; Krafft, M. P. A Nonpolar, Nonamphiphilic Molecule Can Accelerate Adsorption of Phospholipids and Lower Their Surface Tension at the Air/Water Interface. *ChemPhysChem* **2011**, *12* (14), 2646−2652.
(13) Chernyshev, V. S.; Skliar, M. Surface Tension of Water in the Presence of Perfluorocarbon Vapors. *Soft Matter* **2014**, *10* (12), 1937−1943.
(14) Pradines, V.; Fainerman, V. B.; Aksenenko, E. V.; Krägel, J.; Mucic, N.; Miller, R. Adsorption of Alkyl Trimethylammonium Bromides at the Water/Air and Water/Hexane Interfaces. *Colloids Surf. A Physicochem. Eng. Asp.* **2010**, *371* (1−3), 22−28.
(15) Javadi, A.; Moradi, N.; Möhwald, H.; Miller, R. Adsorption of Alkanes from the Vapour Phase on Water Drops Measured by Drop Profile Analysis Tensiometry. *Soft Matter* **2010**, *6* (19), 4710−4714.
(16) Javadi, A.; Moradi, N.; Fainerman, V. B.; Möhwald, H.; Miller, R. Alkane Vapor and Surfactants Co-Adsorption on Aqueous Solution Interfaces. *Colloids Surf. A Physicochem. Eng. Asp.* **2011**, *391* (1), 19−24.
(17) Fainerman, V. B.; Aksenenko, E. V.; Kovalchuk, V. I.; Javadi, A.; Miller, R. Study of the Co-Adsorption of Hexane from the Gas Phase at the Surface of Aqueous C10EO8 Drops. *Soft Matter* **2011**, *7* (17), 7860−7865.
(18) Mys, V. D.; Fainerman, V. B.; Makievski, A. V.; Krafft, M. P.; Miller, R. Dynamic Surface Tension of C10EO8 at the Aqueous Solution/Hexane Vapor Interface as Measured by Bubble Pressure Tensiometry. *Colloids Surf. A Physicochem. Eng. Asp.* **2015**, *483*, 137−141.
(19) Fainerman, V. B.; Aksenenko, E. V.; Kovalchuk, V. I.; Mucic, N.; Javadi, A.; Liggieri, L.; Ravera, F.; Loglio, G.; Makievski, A. V.; Schneck, E.; Miller, R. New View of the Adsorption of Surfactants at Water/Alkane Interfaces - Competitive and Cooperative Effects of Surfactant and Alkane Molecules. *Adv. Colloid Interface Sci.* **2020**, *279*, 102143.
(20) Firooz, A.; Chen, P. Surface Tension and Adsorption Kinetics of Amphiphiles in Aqueous Solutions: The Role of Carbon Chain Length and Temperature. *J. Colloid Interface Sci.* **2012**, *370* (1), 183−191.
(21) Tsarkova, L. A.; Gurkov, T. D. Volatile Surfactants: Characterization and Areas of Application. *Curr. Opin. Colloid Interface Sci.* **2022**, *60*, 101592.
(22) Danov, K. D.; Gurkov, T. D.; Stanimirova, R. D.; Uzunova, R. I. Kinetics of Transfer of Volatile Amphiphiles (Fragrances) from Vapors to Aqueous Drops and Vice Versa: Interplay of Diffusion and Barrier Mechanisms. *Colloids Surf. A Physicochem. Eng. Asp.* **2021**, *625*, 126931.
(23) Uzunova, R. I.; Danov, K. D.; Stanimirova, R. D.; Gurkov, T. D. Quantitative Characterization of the Mass Transfer of Volatile Amphiphiles between Vapor and Aqueous Phases: Experiment vs Theory. *JCIS Open* **2025**, *18*, 100133.
(24) Soboleva, O. A.; Gurkov, T. D.; Stanimirova, R. D.; Protsenko, P. V.; Tsarkova, L. A. Volatile Aroma Surfactants: The Evaluation of the Adsorption-Evaporation Behavior under Dynamic and Equilibrium Conditions. *Langmuir* **2022**, *38* (9), 2793−2803.
(25) Hadji, C.; Dollet, B.; Bodiguel, H.; Drenckhan, W.; Coasne, B.; Lorenceau, E. Impact of Fluorocarbon Gaseous Environments on the Permeability of Foam Films to Air. *Langmuir* **2020**, *36* (44), 13236−13243.
(26) Steck, K.; Dijoux, J.; Preisig, N.; Bouylout, V.; Stubenrauch, C.; Drenckhan, W. Fluorocarbon Vapors Slow down Coalescence in Foams: Influence of Surfactant Concentration. *Colloid Polym. Sci.* **2023**, *301* (7), 685−695.
(27) Qi, N.; Sun, H.; Zhao, H.; Li, Y. Achieving Foaming Control Smartly: Pre-Solubilized Flavor Oil Serves as an in Situ Homogeneous Defoamer. *Soft Matter* **2018**, *14* (11), 2059−2067.
(28) Qi, N.; Chen, Z.; Zhao, H.; Wang, Q.; Chen, H.; Yuan, H.; Li, Y. Predicting and Controlling the Effect of Solubilized Flavor Oil on Foam Properties of Surfactant through Study of the Adsorption Activity and Configuration. *J. Surfactants Deterg.* **2020**, *23* (2), 347−358.
(29) Levich, V. G. *Physicochemical Hydrodynamics*; Prentice-Hall, Inc.: Englewood Cliffs, NJ, 1962.
(30) Sadhal, S. S.; Johnson, R. E. Stokes Flow Past Bubbles and Drops Partially Coated with Thin Films. Part 1. Stagnant Cap of Surfactant Film - Exact Solution. *J. Fluid Mech.* **1983**, *126*, 237−250.
(31) Liao, Y.; McLaughlin, J. B. Bubble Motion in Aqueous Surfactant Solutions. *J. Colloid Interface Sci.* **2000**, *224* (2), 297−310.
(32) Tasoglu, S.; Demirci, U.; Muradoglu, M. The Effect of Soluble Surfactant on the Transient Motion of a Buoyancy-Driven Bubble. *Phys. Fluids* **2008**, *20*, 040805.
(33) Vakarelski, I. U.; Manica, R.; Li, E. Q.; Basheva, E. S.; Chan, D. Y. C.; Thoroddsen, S. T. Coalescence Dynamics of Mobile and Immobile Fluid Interfaces. *Langmuir* **2018**, *34*, 2096−2108.
(34) Zawala, J.; Miguet, J.; Rastogi, P.; Atasi, O.; Borkowski, M.; Scheid, B.; Fuller, G. G. Coalescence of Surface Bubbles: The Crucial Role of Motion-Induced Dynamic Adsorption Layer. *Adv. Colloid Interface Sci.* **2023**, *317*, 102916.
(35) Lotfi, M.; Rajabzadeh Dezfuli, M.; Bastani, D. Evaluation and Prediction of Rise Velocity and Drag Coefficient of an Ascending Bubble Affected by the Impurity in Continuous and Discrete Phases, Distinctly and Concurrently. *Chem. Eng. J.* **2023**, *464*, 142680.
(36) Loglio, G.; Pandolfini, P.; Miller, R.; Makievski, A. V.; Ravera, F.; Ferrari, M.; Liggieri, L. Drop and Bubble Shape Analysis as a Tool For Dilational Rheological Studies of Interfacial Layers. In *Novel Methods to Study Interfacial Layers*; Möbius, D., Miller, R., Eds.; Studies In Interface Science; Elsevier: Amsterdam, 2001; Vol. *11*, pp 439−483.
(37) Para, G.; Jarek, E.; Warszyński, P.; Adamczyk, Z. Effect of Electrolytes on Surface Tension of Ionic Surfactant Solutions. *Colloids Surf. A Physicochem. Eng. Asp.* **2003**, *222*, 213−222.
(38) Para, G.; Jarek, E.; Warszyński, P. The Hofmeister Series Effect in Adsorption of Cationic Surfactants—Theoretical Description and Experimental Results. *Adv. Colloid Interface Sci.* **2006**, *122* (1), 39−55.
(39) Koryta, J.; Dvořák, J.; Boháčková, V. *Lehrbuch Der Elektrochemie*; Springer: Vienna, 1975.
(40) Levine, S.; Robinson, K.; Bell, G. M.; Mingins, J. The Discreteness-of-Charge Effect at Charged Aqueous Interfaces: I.

https://doi.org/10.1021/acs.iecr.5c02608
Ind. Eng. Chem. Res. 2025, 64, 20347−20361

General Theory for Single Adsorbed Ion Species. *J. Electroanal. Chem. Interfacial Electrochem* **1972**, *38* (2), 253−269.
(41) Warszyński, P.; Barzyk, W.; Lunkenheimer, K.; Fruhner, H. Surface Tension and Surface Potential of Na N-Dodecyl Sulfate at the Air-Solution Interface: Model and Experiment. *J. Phys. Chem. C* **1998**, *102*, 10948−10957.
(42) Warszyński, P.; Lunkenheimer, K.; Czichocki, G. Effect of Counterions on the Adsorption of Ionic Surfactants at Fluid-Fluid Interfaces. *Langmuir* **2002**, *18*, 2506−2514.
(43) Borkowski, M.; Batys, P.; Demchuk, O. M.; Kowalczuk, P. B.; Zawala, J. Amino-Acids Surfactants and n-Octanol Mixtures—Sustainable, Efficient, and Dynamically Triggered Foaming Systems. *Ind. Eng. Chem. Res.* **2023**, *62* (34), 13498−13509.
(44) Abraham, M. J.; Murtola, T.; Schulz, R.; Páll, S.; Smith, J. C.; Hess, B.; Lindahl, E. GROMACS: High Performance Molecular Simulations through Multi-Level Parallelism from Laptops to Supercomputers. *SoftwareX* **2015**, *1−2*, 19−25.
(45) MacKerell, A. D., Jr; Bashford, D.; Bellott, M.; Dunbrack, R. L., Jr; Evanseck, J. D.; Field, M. J.; Fischer, S.; Gao, J.; Guo, H.; Ha, S.; Joseph-McCarthy, D.; Kuchnir, L.; Kuczera, K.; Lau, F. T. K.; Mattos, C.; Michnick, S.; Ngo, T.; Nguyen, D. T.; Prodhom, B.; Reiher, W. E.; Roux, B.; Schlenkrich, M.; Smith, J. C.; Stote, R.; Straub, J.; Watanabe, M.; Wiórkiewicz-Kuczera, J.; Yin, D.; Karplus, M. All-Atom Empirical Potential for Molecular Modeling and Dynamics Studies of Proteins. *J. Phys. Chem. B* **1998**, *102* (18), 3586−3616.
(46) Klauda, J. B.; Venable, R. M.; Freites, J. A.; O'Connor, J. W.; Tobias, D. J.; Mondragon-Ramirez, C.; Vorobyov, I.; MacKerell, A. D., Jr; Pastor, R. W. Update of the CHARMM All-Atom Additive Force Field for Lipids: Validation on Six Lipid Types. *J. Phys. Chem. B* **2010**, *114* (23), 7830−7843.
(47) Vanommeslaeghe, K.; Hatcher, E.; Acharya, C.; Kundu, S.; Zhong, S.; Shim, J.; Darian, E.; Guvench, O.; Lopes, P.; Vorobyov, I.; Mackerell, A. D., Jr CHARMM General Force Field: A Force Field for Drug-like Molecules Compatible with the CHARMM All-Atom Additive Biological Force Fields. *J. Comput. Chem.* **2010**, *31* (4), 671−690.
(48) Lee, J.; Cheng, X.; Swails, J. M.; Yeom, M. S.; Eastman, P. K.; Lemkul, J. A.; Wei, S.; Buckner, J.; Jeong, J. C.; Qi, Y.; Jo, S.; Pande, V. S.; Case, D. A.; Brooks, C. L. I.; MacKerell, A. D., Jr; Klauda, J. B.; Im, W. CHARMM-GUI Input Generator for NAMD, GROMACS, AMBER, OpenMM, and CHARMM/OpenMM Simulations Using the CHARMM36 Additive Force Field. *J. Chem. Theory Comput.* **2016**, *12* (1), 405−413.
(49) Izadi, S.; Anandakrishnan, R.; Onufriev, A. V. Building Water Models: A Different Approach. *J. Phys. Chem. Lett.* **2014**, *5* (21), 3863−3871.
(50) Tempra, C.; Ollila, O. H. S.; Javanainen, M. Accurate Simulations of Lipid Monolayers Require a Water Model with Correct Surface Tension. *J. Chem. Theory Comput.* **2022**, *18* (3), 1862−1869.
(51) Bussi, G.; Donadio, D.; Parrinello, M. Canonical Sampling through Velocity Rescaling. *J. Chem. Phys.* **2007**, *126* (1), 014101.
(52) Essmann, U.; Perera, L.; Berkowitz, M. L.; Darden, T.; Lee, H.; Pedersen, L. G. A Smooth Particle Mesh Ewald Method. *J. Chem. Phys.* **1995**, *103* (19), 8577−8593.
(53) Yeh, I.-C.; Berkowitz, M. L. Ewald Summation for Systems with Slab Geometry. *J. Chem. Phys.* **1999**, *111* (7), 3155−3162.
(54) Hess, B.; Bekker, H.; Berendsen, H. J. C.; Fraaije, J. G. E. M. LINCS: A Linear Constraint Solver for Molecular Simulations. *J. Comput. Chem.* **1997**, *18* (12), 1463−1472.
(55) Miyamoto, S.; Kollman, P. A. Settle: An Analytical Version of the SHAKE and RATTLE Algorithm for Rigid Water Models. *J. Comput. Chem.* **1992**, *13* (8), 952−962.
(56) Humphrey, W.; Dalke, A.; Schulten, K. VMD: Visual Molecular Dynamics. *J. Mol. Graph.* **1996**, *14* (1), 33−38.
(57) Martínez, L.; Andrade, R.; Birgin, E. G.; Martínez, J. M. PACKMOL: A package for building initial configurations for molecular dynamics simulations. *J. Comput. Chem.* **2009**, *30* (13), 2157−2164.
(58) Kumar, S.; Rosenberg, J. M.; Bouzida, D.; Swendsen, R. H.; Kollman, P. A. The Weighted Histogram Analysis Method for Free-Energy Calculations on Biomolecules. I. The Method. *J. Comput. Chem.* **1992**, *13* (8), 1011−1021.
(59) Hub, J. S.; de Groot, B. L.; van der Spoel, D. G_wham—A Free Weighted Histogram Analysis Implementation Including Robust Error and Autocorrelation Estimates. *J. Chem. Theory Comput.* **2010**, *6* (12), 3713−3720.
(60) Pfohl, T.; Möhwald, H.; Riegler, H. Ellipsometric Study of the Wetting of Air/Water Interfaces with Hexane, Heptane, and Octane from Saturated Alkane Vapors. *Langmuir* **1998**, *14* (18), 5285−5291.
(61) Campbell, R. A.; Kairaliyeva, T.; Santer, S.; Schneck, E.; Miller, R. Direct Resolution of the Interactions of a Hydrocarbon Gas with Adsorbed Surfactant Monolayers at the Water/Air Interface Using Neutron Reflectometry. *Colloids Interfaces* **2022**, *6* (4), 68.
(62) Zawala, J. Added Mass of Rising Bubble Approaching to Solid Wall - Numerical Studies. *Physicochem. Probl. Miner. Process.* **2020**, *56* (6), 41−50.
(63) Lyttle, D. J.; Lu, J. R.; Su, T. J.; Thomas, R. K.; Penfold, J. Structure of a Dodecyltrimethylammonium Bromide Layer at the Air/Water Interface Determined by Neutron Reflection: Comparison of the Monolayer Structure of Cationic Surfactants with Different Chain Lengths. *Langmuir* **1995**, *11* (3), 1001−1008.
(64) Kowalczuk, P. B.; Zawala, J.; Drzymala, J. Concentration at the Minimum Bubble Velocity (CMV) for Various Types of Flotation Frothers. *Minerals* **2017**, *7* (7), 118.
(65) Tate, T. On the Magnitude of a Drop of Liquid Formed under Different Circumstances. *Philos. Mag.* **1864**, *27*, 176−180.
(66) Legendre, D.; Zenit, R.; Velez-Cordero, J. R. On the Deformation of Gas Bubbles in Liquids. *Phys. Fluids* **2012**, *24* (4), 043303.
(67) Moore, D. W. The Velocity of Rise of Distorted Gas Bubbles in a Liquid of Small Viscosity. *J. Fluid Mech.* **1965**, *23*, 749−766.
(68) Loth, E. Quasi-Steady Shape and Drag of Deformable Bubbles and Drops. *Int. J. Multiph. Flow* **2008**, *34* (6), 523−546.
(69) Nguyen, A. V. Prediction of Bubble Terminal Velocities in Contaminated Water. *AIChE J.* **1998**, *44*, 226−230.
(70) Wang, J.; Pang, M.; Lv, F. Effect of Adsorption Dynamics on Hydrodynamic Characteristics of a Bubble Contaminated by Surfactants at Medium Reynolds Numbers. *Microgravity Sci. Technol.* **2022**, *34* (3), 36.

https://doi.org/10.1021/acs.iecr.5c02608
Ind. Eng. Chem. Res. 2025, 64, 20347−20361